

# Identification of Chimera using Machine Learning

M.A. Ganaie<sup>1</sup>, Saptarshi Ghosh<sup>2</sup>, Naveen Mendola<sup>2</sup>, M Tanveer<sup>1</sup> & Sarika Jalan<sup>2,3,\*</sup>

<sup>1</sup> *Discipline of Mathematics, Indian Institute of Technology Indore, Khandwa Road, Simrol, 453552 Indore India*

<sup>2</sup> *Complex Systems Lab, Discipline of Physics, Indian Institute of Technology Indore, Indore 452017, India*

<sup>3</sup> *Discipline of Biosciences and Biomedical Engineering, Indian Institute of Technology Indore, Indore 452017, India*

\* *E-mail: sarikajalan9@gmail.com*

## Abstract

Coupled dynamics on the network models have been tremendously helpful in getting insight into complex spatiotemporal dynamical patterns of a wide variety of large-scale real-world complex systems. Chimera, a state of coexistence of incoherence and coherence, is one of such patterns arising in identically coupled oscillators, which has recently drawn tremendous attention due to its peculiar nature and wide applicability, specially in neuroscience. The identification of chimera is a challenging problem due to ambiguity in its appearance. We present a distinctive approach to identify and characterize the chimera state using machine learning techniques, namely random forest, oblique random forests via multi-surface proximal support vector machines (MPRaF-T, P, N) and sparse pre-trained / auto-encoder based random vector functional link neural network (RVFL-AE). We demonstrate high accuracy in identifying the coherent, incoherent and chimera states from given spatial profiles. We validate this approach for different time-continuous and time discrete coupled dynamics on networks. This work provides a direction for employing machine learning techniques to identify dynamical patterns arising due to the interaction among non-linear units on large-scale, and for characterizing complex spatio-temporal phenomena in real-world systems for various applications.

The identification and characterization of chimera state in various complex dynamical systems is a challenging but essential task, given its new-found applicability in various areas. Recently, machine learning (ML) techniques have demonstrated tremendous promise in various areas of nonlinear dynamics and network science. Here, we present a universal machine learning-based approach towards the identification of chimera states by utilizing five ML algorithms, namely RaF, MPRaF-T, P, N, and RVFL-AE, trained on mere dynamical spatial configurations as input. This technique can characterize different dynamical states and identify chimera patterns in various time-discrete and time-continuous model systems.

## 1 Introduction

In 2002, Kuramoto and Battogtokh [1] reported a strange co-existence of phase locked and drifting oscillators in non-locally coupled network of identical oscillators. Later on, Abrams and Strogatz christened the state as the chimera state after a fire-breathing hybrid monster from Greek mythology and provided a mathematical foundation to its appearance [2]. Since then, the chimera state has been reported to occur in numerous complex systems ranging from network of opto-electronic oscillators [3] to brain [4,5], leading to a wide deviation from the initial definition and stringent conditions proposed

by Kuramoto et.al. and Abrams et.al. in their landmark papers. Its exotic nature and appearance in a wide variety of real-world complex systems lead to an explosive interest in chimera, yielding a huge literature in theoretical [6–12] as well as experimental [13–16] investigations. However, the chimera state reported for a diverse range of systems, manifest into diverse forms in terms of variations in shape, appearances, mobility, spatio-temporal behavior and many more [17, 18]. Chimeras has been dubbed as spatio-temporal phenomenon mostly in time-continuous systems [1, 2] whereas time-discrete maps [6, 7] primarily exhibit chimera state with only spatial chaos with simple temporal behavior (mostly periodic). A third type of chimera state has also been reported with both temporal as well as spatial chaotic behavior [19]. For example, an amplitude chimera corresponds to the coexistence of coherent and incoherent behavior in amplitude with all oscillators possessing the same average frequency [20]. Breathing chimera states correspond to periodic appearance of the state, whereas in travelling chimera state, the incoherent part is non-static in time [21–23]. In addition to previously reported chimera in 1D (regular) networks, chimera state has been reported for 2D [24, 25] and 3D [26, 27], systems as well. Additionally, both local [8, 28] and global coupling [29] schemes have been shown to yield a chimera state.

Overall, the field of chimera state has broaden quite a lot in different areas in past-few years. Due to this disparate expansion, identification and classification of a chimera site has become a huge challenge. A plethora of measures has been proposed towards the same goal. Kemeth et al. reported a generalized Laplacian correlation measure to classify different types of chimera states [31]. Gopal et al. presented the strength of incoherence and the discontinuity measure to identify single and multi-chimera state for the underlying parameter space [32]. Furthermore, a local order parameter has been widely used to identify chimera states in phase oscillators [33, 34]. Hizanidis et al. presented a chimera-like and metastability indices to recognize chimera states [35]. However, recent surge in finding new applications of chimera state calls for a universal method to identify chimera state without any numerical restrictions as well as regardless of the underlying complex nature of the considered model.

This article embarks on a very distinct approach to propose a efficient method to identify chimera states using machine learning technique. Significant advances have been made in the field of machine learning, leading to its extensive usage in diverse fields ranging from Astro-Physics to natural language recognition, image processing to bio-medical applications [36, 37]. Recently, a series of literature related to the implementation of machine learning techniques into non-linear dynamics, has emerged. The recent surge in exploiting machine learning techniques in the investigation of complex dynamical behavior from *reconstruction of attractor of chaotic dynamical systems* [38, 39] or *hybrid forecasting of chaotic processes* [40] to *predicting dynamical observable from network structure* [41], has initiated a new approach to address well-known research problems in nonlinear dynamics. Previously, machine learning techniques have been used to analyse complex spatio-temporal patterns in coupled dynamical systems [42, 43].

This article uses multiple machine learning models to identify the chimera states. Based on the recent survey [44], random forests (RaF) [45] emerged as the best classifier. We used Random forest and its ensembles [46] as the classification models. The ensembles of the RaF (MPRaF-T, P, N) are based on the different regularization techniques used in the multisurface proximal support vector machine (MPSVM). At each node of the decision trees, MPSVM generates the oblique split hyperplane based on the multiple features of the data. Unlike RaF, MPSVM based oblique random forests capture the geometric structure of the data and hence show better performance. Moreover, we also used sparse pre-trained functional link network [47], also known as auto-encoder based RVFL network (RVFL-AE), to learn an efficient feature representation of the data based on the  $l_1$  norm regularized autoencoder. Autoencoder explores the hidden feature information which help in the better performance of the model [47].

Here, we employ five advanced machine learning (ML) algorithms, namely RaF, MP RaF-T, MP RaF-P, MP RaF-N and RVFL-AE, to identify chimera states from underlying spatial data, and argue that, due to the generalized approach and adaptive nature of the methods, they can be easily applied to find co-existing patterns for given parameter ranging from amplitude or frequency data of phase oscillators to electrode data from EEG readings. With the help of four different coupled dynamics namely Kuramoto Oscillators and FitzHughNagumo oscillators for time-continuous and coupled Logistic map and Heñon map for time-discrete dynamics on network of identical couplings i.e. a regular network, we validate ML algorithms in recognizing the complex spatio-temporal patterns and demonstrate a high accuracy rate in categorizing them in chimera, coherent and incoherent states. Table 2 shows that most of the machine learning models show competitive performance for identifying the chimera states. One can see that all the machine models RaF, MP RaF-T, MP RaF-P, MP RaF-N and RVFL-AE show 87.8% accuracy in Model-Kuramoto Osc. In Model-Logistic-Map, RaF and MP RaF-T showed 90% accuracy while as in Model-Henon-Map and Model-FHN Osc MP RaF-N shows 85.3% accuracy and 78.1% accuracy, respectively.

The paper is organized as follows. After the first introductory section containing motivation, research gap as well as the proposed plan, we discuss various machine learning techniques employed by us in the second section. The third section contains the results as well as discusses their implications. The fourth section concludes the work followed by a section discussing future directions.

## 2 Machine Learning Techniques

In this section, we elaborate the five Machine Learning algorithms (RaF, MP RaF-T, MP RaF-P, MP RaF-N and RVFL-AE) that have been used in this investigation for identification and characterization of the spatial patterns.

### 2.1 Random Forest

Originally given by Breiman [45], random forest is an ensemble of decision trees based on the concept of bagging and random subspaces. Each decision tree of the RaF is trained on the randomly initialized vectors sampled independently with same distribution of the original training dataset. Combining the concepts of bagging and random subspaces leads to the increase of variance among the base classifiers. Each decision tree generated on the bootstrapped version of the training data evaluates the “*mtry*” number of random subspace features to chose the best split based on the impurity gain. The “*mtry*” parameter determines the number of split tests at each non-leaf node of the tree. The feature which optimizes the impurity gain is chosen as the best split. The details of RaF are given in Algorithm 1.

---

**Algorithm 1** Random Forest Algorithm [45]

---

Training Phase:

Given:

$P = M \times n$  is the training data with  $M$  number of samples each of dimension  $n$ .

$Q = M \times 1$  are labels of the training data.

$R$  represents the ensemble size i.e. number of trees.

Each tree in the random forest is represented as  $T_i$ , where  $i = 1, \dots, R$ .

“ $mtry$ ” is the number of randomly selected subset of features.

“ $minleaf$ ” is the maximum number of samples in an impure node.

1. Each tree  $T_i$  is build using the bootstrapped versions of the training data  $P$  with replacement.
2. At each non-leaf node, the best feature split is selected among the “ $mtry$ ” randomly selected features from the training data.
3. Repeatedly execute step 2 until one of the conditions is met:
  - Node becomes pure.
  - Node contains number of samples less than or equal to  $minleaf$ .

Classification Phase:

For each testing sample, each tree in the forest assigns the vote to the given sample data. Then based on the maximum voting, each data sample is assigned a class.

---

## 2.2 Oblique Random Forest via MPSVM

RaF generates the decision trees based on the evaluation of features at each node of the tree and the final split occurs with the single feature that improves the purity of the node. However, single feature based decision trees may not be optimal as they fail to capture the geometric structure of the data. To overcome this limitation, oblique decision tree ensemble via MPSVM [46] was proposed. Here, splitting at each node is based on the hyperplanes generated via multisurface proximal support vector machines (MPSVM). These hyperplanes capture the geometric structure of the data and hence show better performance as compared to the RaF. However, MPSVM is originally designed for binary class problems. Hence, Algorithm (2) is used to handle the multiclass problems. In this Algorithm 2, Bhattacharyya distance is used to obtain the groups of maximum distance. The Bhattacharyya distance between the normal classes  $L_j$  and  $L_k$ ,  $N(\mu_j, \sum_j)$  and  $N(\mu_k, \sum_k)$ , is given as

$$B(L_j, L_k) = \frac{1}{8}(\mu_k - \mu_j)^T \left( \frac{\sum_j + \sum_k}{2} \right)^{-1} (\mu_k - \mu_j) + \frac{1}{2} \ln \frac{|(\sum_j + \sum_k)/2|}{\sqrt{|\sum_j| |\sum_k|}}. \quad (1)$$

---

**Algorithm 2** Multiclass to Binary class [46]

---

**Input:**

$P = M \times n$  is the training data with  $M$  number of samples each of dimension  $n$ .

$Q = M \times 1$  are labels of the training data.

$\{L_1, \dots, L_c\}$  is the set of data labels.

**Output:**  $G_p$  and  $G_n$  are the two hyperclasses or groups.

- 1: **for**  $j = 1, \dots, c$  **do**
  - 2:     Calculate the Bhattacharyya distance between every pair of classes  $L_j$  and  $L_k$ , with  $k = j + 1, \dots, c$  using equation (1).
  - 3: **end for**
  - 4: Chose classes  $L_p$  and  $L_n$  such that  $L_p$  and  $L_n$  are at largest Bhattacharyya distance, put them in groups  $G_p$  and  $G_n$  respectively.
  - 5: For every other class, if  $B(L_k, L_p) < B(L_k, L_n)$  then assign the  $L_k$  to the group  $G_p$  else put in group  $G_n$ .
- 

The matrices appearing in the formulation of MPSVM are positive semi-definite. To handle this singularity problem in MPSVM formulation, different regularization techniques are used: 1) Tikhonov regularization [48] and 2) axis-parallel split regularization [49, 50] 3) Null Space regularization [51]. In Tikhonov regularization method, small constant is added to the diagonal entries of the matrix to be regularized. Suppose  $G$  is rank deficient then  $G$  is regularized as

$$G' = G + \delta \times I. \quad (2)$$

while as in axis-parallel split regularization, if a matrix becomes singular, then axis parallel split is used to continue the generation of a tree. In Null space regularization method, orthogonal projections are used for regularization. Based on the different approaches used to handle the singularity problem, the classification models are named accordingly. MPraF-T, MPraF-P, and MPraF-N represent the MPSVM-based RaFs with Tikhonov, axis-parallel, and NULL space regularization, respectively.

### 2.3 Sparse Pre-Trained Random Vector Functional Link (SP-RVFL) network

Sparse Pre-Trained Random Vector Functional Link (SP-RVFL) network is an unsupervised network parameter learning paradigm [47]. In this method, sparse autoencoder with  $l_1$  norm regularization is used to learn the network parameters instead of the random weights of RVFL [52]. The sparse autoencoder leads to more informative features which are retained for the subsequent learning of the feature representation. The SP-RVFL shows better performance as compared to the standard RVFL network [47]. The weights learned by the model in the autoencoder are used to initialize the hidden layer weights of the SP-RVFL model. The weights in the output layer of the model are optimized via closed form solution. For more details, interested readers are referred to [47].

## 3 Result and Discussions

This article aims at characterizing different dynamical states using machine learning algorithms described in previous section. We divide the validation of the algorithms into four parts where we consider two time-discrete and two time-continuous dynamical models to generate the required data

for training and testing. It should be noted that the data used for training and testing the dynamical models is primarily the snapshot profile i.e., a  $[N \times 1]$  vector, representing the state of the model, at a particular time-step in the steady state with  $N$  being the size of network. Although, in some cases the frequency or the amplitude is used to discern the chimera and other states, the use of snapshot profile enables us to perform a generalized approach, regardless of the time-continuous or time discrete nature of the considered system. We argue that because of the approach undertaken in the manuscript, this novel technique can be universally applicable to any coupled dynamics and real-world time series data, where chimera patterns are destined to emerge.

In the following, we first briefly describe the chimera and other states followed by a demonstration of the state for different dynamical models. Chimera state is described as an exotic state where coherent and incoherent dynamics co-exist with each other in a network of identical oscillators. We considered an undirected single-layer regular network (S 1 : ring), where all the  $N$  nodes have same degree  $k$ . The node degree is also represented as coupling radius defined as  $r = k/2N$ . The interaction pattern of the nodes in the network is encoded by an adjacency matrix  $\mathcal{A}$  such that  $a_{ij} = 1$ , if a link exists between nodes  $i$  and  $j$ , and zero, otherwise.

Formally, we define the existence of coherence in the snapshot profile of coupled dynamical model on a networks as [7]

$$\lim_{N \rightarrow \infty} \lim_{t \rightarrow \infty} \sup_{i,j \in U_\xi^N(x)} |z_i(t) - z_j(t)| \rightarrow 0 \text{ for } \xi \rightarrow 0 \quad (3)$$

where  $U_\xi^N(x) = \{j : 0 \leq j \leq N, | \frac{j}{N} - x | < \xi\}$  represents the network neighborhood of any point  $x \in S^1$ , i.e., of the regular network. The  $\mathbf{Z}(t) \in \mathbb{R}^N$  represents the state vector ( $N \times 1$ ) with the components  $z_i(t) \ni \mathbf{Z} = \{z_1, z_2, \dots, z_N\}$ , as a real dynamical variable at time  $t$  for the  $i^{th}$  node for the considered model.  $N$  stands for the number of nodes in the network and hence the adjacency matrix is of dimension  $N \times N$  and the state vector is of dimension  $N \times 1$ . In the asymptotic limit ( $N \rightarrow \infty$ ),  $\mathbf{Z}^t$  approaches a smooth spatial profile for a coherent state without any discontinuity in the spatial profile. On the other hand, the spatial profile of an incoherent state does not show any smooth segment in the snapshot. A chimera, which comprises of coexisting coherent and incoherent states, shows smooth profiles broken by non-smooth segments, representing discontinuities in the snapshot. A detailed discussion can be found in Ref. [53]. In the following, we describe the governing equation for time evolution of the state vector belong to different dynamical models with the regular single-layer undirected network.

### 3.1 Coupled Kuramoto Oscillators

The pragmatic Kuramoto model [54, 55] represents one of most explored coupled dynamical model which is simplistic in nature, yet capable of showing complex dynamical phenomena. A plethora of research has been done towards demonstrating its applicability in diverse areas of research [56] including the chimera, for which, the emergence of chimera is initially reported [1].

The state vector for the kuramoto model is defined in terms of the phases ( $\theta$ ) of  $N$  nodes of the network. Therefore,  $\Theta = \theta_1, \theta_2, \dots, \theta_N$  represents the dynamical state of the system at a particular time, representing the phase of each node as a real variable  $\theta_i \in \mathbb{R}, \forall i = 1, \dots, N$ . The governing equation for kuramoto model utilizing the adjacency matrix can be written as [57]

$$\dot{\theta}_i = \omega_i - \frac{\lambda}{\sum_j a_{ij}} \sum_{j=1}^N a_{ij} \sin(\theta_j - \theta_i + \alpha) \quad (4)$$

where  $\lambda$  denotes the coupling strength,  $\omega_i = \omega; \forall i$  denotes the constant natural frequency of all oscillators and  $\alpha$  denotes a constant phase lag. We chose all the system parameters, namely,  $\alpha$  and

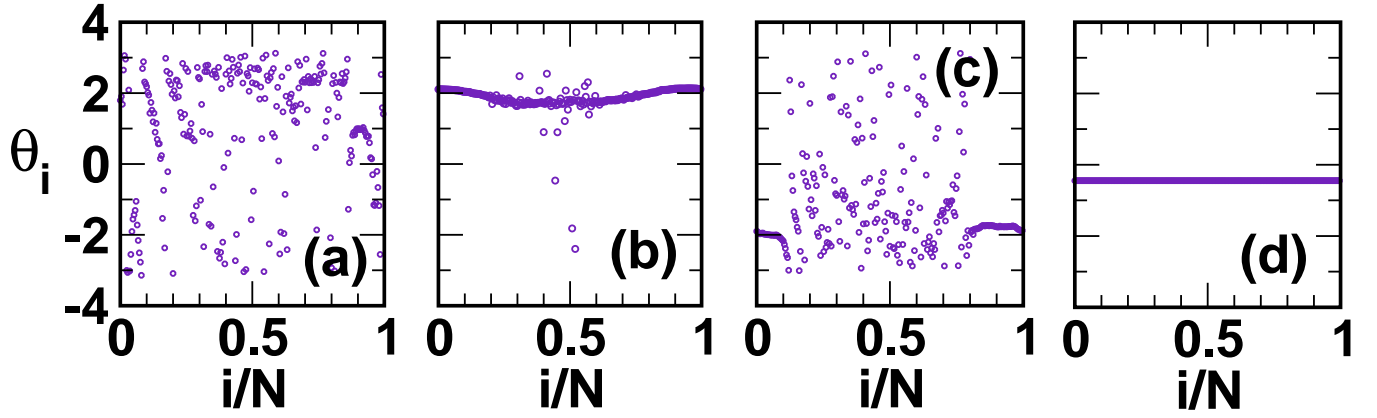


Figure 1: Snapshots of phase-state of non-locally kuramoto oscillators arranged in a regular network  $A(N, r)$  demonstrating (a) incoherent state for  $\alpha = 1.65$ , (b) Chimera state for  $\alpha = 1.4$ , (c) Chimera state for  $\alpha = 1.5$ , and (d) Incoherent state  $\alpha = 0.2$ . Other parameters are  $N = 250, r = 0.32, \lambda = 0.1, \omega_i = \omega = 0.01, \forall_i$ .

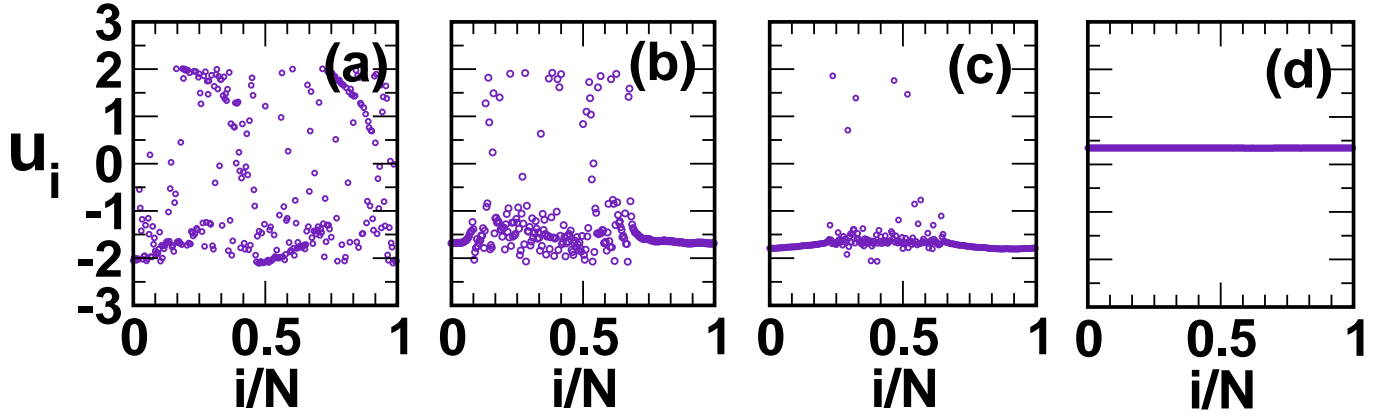


Figure 2: Snapshot profiles of activator variable of non-locally coupled FHN oscillators arranged in a regular network  $A(N, r)$  demonstrating (a) Incoherent state for  $\phi = \pi/2 + 0.35$ , (b) Chimera state for  $\phi = \pi/2 - 0.1$ , (c) Chimera state  $\phi = \pi/2 - 0.15$ , and (d) Coherent state  $\phi = \pi/2 - 0.35$ . Other parameters are  $N = 300, r = 0.35, \lambda = 0.1, a = 0.5, \varepsilon = 0.05$ .

$\lambda$  as well as use a specially constructed initial condition, such that varying the value of the phase lag parameter  $\alpha$  gives rise to different dynamical states. Fig. 1 depicts different dynamical states arising from the choice of the phase lag parameter  $\alpha$ . Note that Figs. 1 (b) and (c) demonstrating chimera states, comprise of smooth segments broken by an incoherent regions, whereas Fig. 1 (a) does not have a smooth segment denoting an incoherent profile and Fig. 1 (d) shows a completely smooth profile representing a coherent state.

### 3.2 Coupled FitzHugh-Nagumo (FHN) Oscillators

Next, we consider FitzHugh-Nagumo (FHN) model which has been a famous model for neural excitability [58]. This two-dimensional coupled dynamical system demonstrates chimera states for isolated networks consisting of coupled oscillatory [34] and excitatory [59] FHN systems. The governing

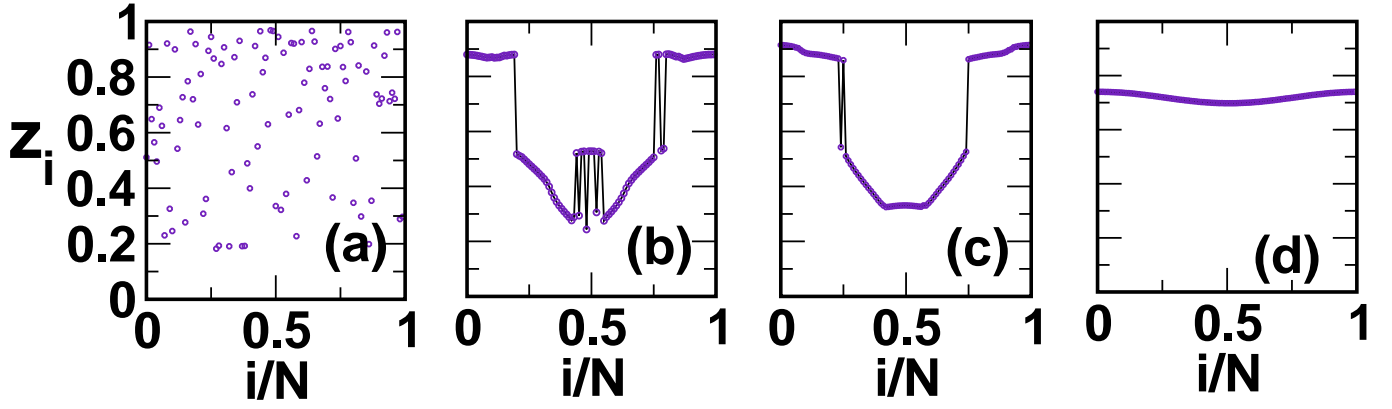


Figure 3: Snapshot profiles of state variable of non-locally coupled logistic map arranged in a regular network  $A(N, r)$  demonstrating (a) Incoherent for  $\varepsilon = 0.1$ , (b) Chimera state for  $\varepsilon = 0.34$ , (c) Chimera state for  $\varepsilon = 0.37$ , and (d) Coherent state for  $\varepsilon = 0.7$ . Other parameters are  $N = 100$ ,  $r = 0.32$ ,  $\mu = 4.0$ .

equation for this model can be described as [60]

$$\begin{aligned} \varepsilon \frac{du_i}{dt} &= u_i - \frac{u_i^3}{3} - v_i + \frac{\lambda}{\sum_j a_{ij}} \sum_{j=1}^N a_{ij} \{ b_{uu}(u_j - u_i) \\ &\quad + b_{uv}(v_j - v_i) \}, \\ \frac{dv_i}{dt} &= u_i + a + \frac{\lambda}{\sum_j a_{ij}} \sum_{j=1}^N a_{ij} \{ b_{vu}(u_j - u_i) \\ &\quad + b_{vv}(v_j - v_i) \}, \end{aligned} \quad (5)$$

The state vector of this model can be described by two variables namely  $u_i$  and  $v_i$ , which represent the activator and inhibitor variables, respectively. A small parameter responsible for the time scale separation of fast activator and slow inhibitor is given by  $\varepsilon > 0$ . Here we fix  $\varepsilon = 0.05$ . System parameter  $a$  defines the excitability threshold. For a single FHN unit it decides between the excitable state for ( $|a| > 1$ ), or the oscillatory state for ( $|a| < 1$ ). Here, we consider the oscillatory regime and fix  $a = 0.5$ . Furthermore, the FHN model, considered here, includes direct as well as cross couplings between activator  $u_i$  and inhibitor  $v_i$  variables, which is encoded by a rotational coupling matrix [60]

$$B = \begin{pmatrix} b_{uu} & b_{uv} \\ b_{vu} & b_{vv} \end{pmatrix} = \begin{pmatrix} \cos\phi & \sin\phi \\ -\sin\phi & \cos\phi \end{pmatrix}. \quad (6)$$

Different dynamical states for the model can be demonstrated by choosing different rotation angle  $\phi$  for the coupling matrix as depicted in Fig. 2. Figs. 2 (a) and (d) show a coherent and incoherent state, respectively for different values of the rotating angle  $\phi$  keeping other system parameters the same. Chimera state demonstrated in Fig. 2 (b) and (c) for such systems has been previously reported in Ref. [34]. For detailed explanation on the choice of the systems parameters can be found in Ref. [60].

### 3.3 Coupled Logistic Map

Next, we consider the logistic map model as local dynamical system, represented by  $f(z) = \mu z(1 - z)$  where the state variable  $z \in [0, 1]$  [61]. We have considered the map in its chaotic regime and therefore set the bifurcation parameter  $\mu = 4.0$  [62]. This simplistic model has been thoroughly explored in the



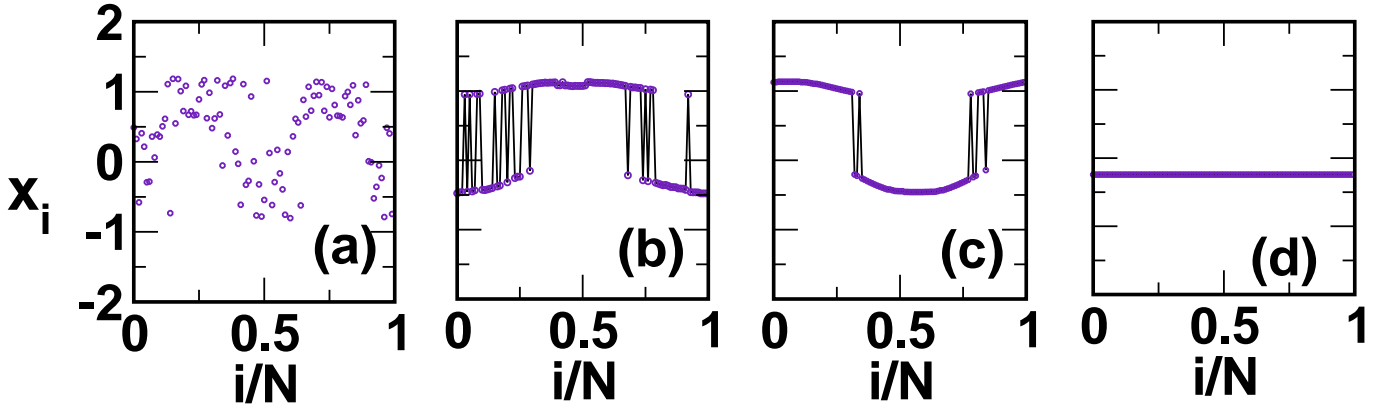


Figure 4: Snapshot profiles of  $x$  state variable of non-locally coupled Hénon map arranged in a regular network  $A(N, r)$  demonstrating (a) Incoherent state for  $\varepsilon = 0.1$ , (b) Chimera state for  $\varepsilon = 0.26$  (c) Chimera state for  $\varepsilon = 0.3$ , and (d) Coherent state for  $\varepsilon = 0.7$ . Other parameters are  $N = 100$ ,  $r = 0.32$ ,  $\alpha = 1.4$ ,  $\beta = 0.3$ .

non-linear dynamics community to understand diverse spatio-temporal phenomena in a wide range of real world networks [63] among which chimera has also been shown in both single [7] and multiplex networks [6]. The dynamical evolution of the coupled logistic map model is governed by

$$z_i^{t+1} = f(z_i^t) + \frac{\varepsilon}{\sum_j a_{ij}} \sum_{j=1}^N a_{ij} [f(z_j^t) - f(z_i^t)] \quad (7)$$

where  $\varepsilon \in [0, 1]$  depicts the overall coupling strength and  $\sum_j a_{ij}$  is the normalizing factor. Depending on the coupling strength  $\varepsilon$  value, different dynamical states can arise for the coupled logistic map model as shown in Fig.3. Figs.3 (b) and (c) report chimera state for mid-range coupling strength [6,7] whereas Fig.3 (a) and (d) demonstrate incoherent and coherent state for low and high coupling strength, respectively.

### 3.4 Coupled Hénon Map

Finally, we consider another pragmatic time-discrete model known as Hénon planner map [64] represented as  $f(x_i^t, y_i^t) = 1 - \alpha(x_i^t)^2 + y_i^t$ . Here also, we set the system parameters  $\alpha = 1.4$  and  $\beta = 0.3$  to obtain chaotic local dynamics. This map represents a well-studied coupled dynamical system which is known to show complex chaotic behavior including emergence of hybrid spatio-temporal patterns of chimera state [12]. The time evolution of the map along with the adjacency matrix can be described as [53]

$$\begin{aligned} x_i^{t+1} &= f(x_i^t, y_i^t) + \frac{\varepsilon}{\sum_j a_{ij}} \sum_{j=1}^{2N} C_{ij} [f(x_j^t, y_j^t) - f(x_i^t, y_i^t)] \\ y_i^{t+1} &= \beta x_i^t \end{aligned} \quad (8)$$

Here,  $\varepsilon \in [0, 1]$  presents the overall coupling strength and  $\sum_j a_{ij}$  is the normalizing factor. Similarly as in the case of logistic map, the choice of the value of coupling strength  $\varepsilon$  causes different dynamical states to arise in coupled hénon map model as shown in Fig.4. Figs.4 (b) and (c) show chimera state for mid-range coupling strength [12] and Fig.4 (a) and (d) demonstrate incoherent and coherent state for low and high coupling strength, respectively.

Model	RVFL-AE	RaF	MPRaF-T	MPRaF-P	MPRaF-N
Model-Kuramoto Osc	80.2	82	89.5	84.5	90
Model-Logistic-Map	61.7	70	73	71	67
Model-Hennon-Map	87.3	96	99	96	99
Model-FHN Osc	100	99	100	99	100

Table 1: Prediction Accuracy (%) for the training data corresponding to different models by different classifier algorithms

### 3.4.1 Numerical setup

The different parameters corresponding to different models were set as follows: the number of trees in each forest is 100 for RaF, MPRaF-T, MPRaF-P and MPRaF-N, the regularization parameter in MPSVM,  $\delta = 0.01$  and the number of hidden neurons for RVFL-AE was chosen from the range 2 : 20 : 302.

### 3.4.2 Training

We show that the ML algorithm identifies the chimera patterns for all the dynamical models and thus establishes the universality of the proposed technique. We first simulate the model system described in the previous section such that they demonstrate coherent, chimera and incoherent states for the suitable chosen initial condition and the system’s parameters. We chose the snapshot profiles to train and test our data for different models. The parameter setting corresponding to different machine learning models while training, are given in above subsection.

### 3.4.3 Prediction Accuracy corresponding to chimera states

We have trained the ML algorithm using the dynamical states as input and trained to classify the states into three categories namely coherent, incoherent and chimera states. The results given in Table 1 represent the average accuracy obtained for 5-times four fold cross validation technique for the training data. One can see from the Table (1), all models perform better on the Model-FHN Osc and Model-Hennon-Map except RVFL-AE on Model-Hennon-Map which shows relatively lower performance. The performance of MPRaF-N model on Model-Kuramoto Osc is better and that of RVFL-AE is relatively poor as compared to the other models. In Model-Logistic-Map, MPRaF-T (with 73% accuracy) performs better as compared to the other baseline models.

Table (2) represents the classification accuracy, sensitivity and specificity measures corresponding to the test data. In Model-Kuramoto Osc, all the models achieved 87.8% accuracy. In Model-Logistic-Map, RVFL-AE shows lower performance as compared to the other given models, however, RaF and MPRaF-T achieved 90% accuracy while MPRaF-N shows 80.2% accuracy. In Model-Hennon-Map, MPRaF-N and MPRaF-T achieved relatively better accuracy (85.3% and 82.1% respectively) as compared to the RaF and MPRaF-P models which showed 75.8% and 77.9% accuracy, respectively. However, RVFL-AE shows lower performance (46.3% accuracy) as compared to the other baseline models. In Model FHN Osc, MPRaF-N shows relatively better performance (78% accuracy) followed by MPRaF-T with 72.9% and RaF with 71.8% accuracy. RVFL-AE and MPRaF-P achieved around 70% accuracy. The sensitivity and specificity measures of different machine learning algorithms in different models corresponding to coherent, incoherent and chimera classes are also given Table (2).

From the above analysis, one can conclude that the MPRaF-T, P, N showed consistent performance while as the performance of RVFL-AE varied in each model and showed lower performance

Model-Kuramoto Osc							
Discarded=1		Sensitivity			Specificity		
Algorithm	Accuracy	coherent	incoherent	chimera	coherent	incoherent	chimera
MPRaF-N	0.8788	1	0	0	0	1	1
MPRaF-P	0.8788	1	0	0	0	1	1
MPRaF-T	0.8788	1	0	0	0.25	1	0.9677
RaF	0.8788	1	0	0	0	1	1
RVFL-AE	0.8788	1	0	0	0	1	1
Model-Logistic-Map							
Discarded=10		Sensitivity			Specificity		
Algorithm	Accuracy	coherent	incoherent	chimera	coherent	incoherent	chimera
MPRaF-N	0.8022	0.86	0.5217	1	0.9756	1	0.7671
MPRaF-P	0.8681	0.82	0.9565	0.8889	1	0.8824	0.9452
MPRaF-T	0.9011	0.86	1	0.8889	1	0.9706	0.9041
RaF	0.9011	0.86	0.9565	0.9444	1	0.9853	0.8904
RVFL-AE	0.6703	0.8	0.4348	0.6111	0.6829	0.8676	0.8904
Model-Hennon-Map							
Discarded=6		Sensitivity			Specificity		
Algorithm	Accuracy	coherent	incoherent	chimera	coherent	incoherent	chimera
MPRaF-N	0.8526	1	0.95	0.4348	0.7674	0.96	0.9861
MPRaF-P	0.7789	0.7885	0.85	0.6957	0.8837	0.8667	0.9167
MPRaF-T	0.8211	1	0.9	0.3478	0.7209	0.96	0.9722
RaF	0.7579	0.75	0.8	0.7391	0.8605	0.9067	0.8611
RVFL-AE	0.4632	0.4038	0.55	0.5217	0.8605	0.6133	0.7778
Model-FHN Osc							
Discarded=3		Sensitivity			Specificity		
Algorithm	Accuracy	coherent	incoherent	chimera	coherent	incoherent	chimera
MPRaF-N	0.7813	1	1	0.5435	0.8028	0.9014	1
MPRaF-P	0.7083	1	1	0.3913	0.6479	0.9577	1
MPRaF-T	0.7292	1	1	0.4348	0.662	0.9718	1
RaF	0.7188	1	1	0.413	0.6338	0.9859	1
RVFL-AE	0.6979	1	1	0.3696	0.5915	1	1

Table 2: Prediction Accuracy (%), sensitivity and specificity for the test data corresponding to different models by different classification algorithms

in all the models except Model-Kuramoto Osc wherein all the given classification models achieved 87.8% accuracy. Note that, we have discarded the disputed states while computing the success rate of the algorithms.

## 4 Conclusion

To summarize, we have employed several machine learning techniques to characterize different dynamical states arising due to the interaction between its constituent entities with a special focus on chimera states. We have used two time-discrete and two time-continuous models to validate our approach and found that the algorithms are quite successful in characterizing the emergent states into chimera coherent and incoherent states. A point to note here that, all selected models are well represented in literature to display chimera states. Here, we use them as a platform to demonstrate the utility of machine learning approach to advance the automated characterization of the emergent dynamics. We have demonstrated that different algorithms showed varying performance based on the dynamical states used. The identification of states in Model-Kuramoto Osc and Model-Logistic-Map by classification models (except RVFL-AE on Model-Logistic map) achieved more than 80% accuracy. However, the performance of algorithms (RaF, MP RaF-T, and MP RaF-P) achieved relatively lower performance (with more than 70% accuracy) on Model-Henon-Map and Model-FHN Osc as compared to their performance in other two given models.

## 5 Future Perspectives

This investigation demonstrates the use of the machine learning algorithms to identify complex spatio-temporal patterns which can help in understanding emergence of such patterns in large scale real-world complex systems.

For example, chimera state has been found to play a crucial role in cognitive functions in human brains [4]. Electroencephalogram (EEG) readings at the onset of epileptic seizure is reported to show chimera-like patterns [30]. However, the identification measures present in literature, being designed in a model-specific way, lacks the universal applicability for the task as well as may require additional threshold criteria to correctly identify chimera state. Our simplistic approach based on the machine learning techniques demonstrate high accuracy rate in identifying and characterizing such spatial patterns, providing new ways to diagnose various neural disorders associated with such patterns. Moreover, our approach is not only limited to characterization of chimera patterns. Diverse emergent dynamics of various coupled complex systems exhibit a plethora of novel spatio-temporal patterns, resulting in diverse applications in various fields ranging from power grid to social systems. For example, cluster synchronization (CS), which represents a dynamic division of a network in two or more different groups of synchronized oscillators, very commonly emerges in neural, social and many other real-world systems represented by networks [67–70]. Therefore, ML techniques presented in the article may also help in automated identification and characterization of dynamical patterns arising in coupled dynamics on networks for various applications.

## Acknowledgments

SJ acknowledges DST project grant (EMR/2016/001921) and CSIR project grant (25 (0293)/18/EMR - II) for financial support. SG acknowledges DST for the INSPIRE fellowship (IF150149).

## Code and Sample Data Files availability:

All codes used in the present article along with the sample files for the figures are publicly available on GitHub Repo at following url: [https://github.com/complex-systems-lab/Project\\_Chimera\\_ML/tree/master](https://github.com/complex-systems-lab/Project_Chimera_ML/tree/master)

## References

- [1] Y. Kuramoto, D. Battogtokh, Nonlinear Phenomena in Complex Systems, **5(4)**, 380385 (2002).
- [2] D.M. Abrams, S. H. Strogatz, Physical review letters **93(17)**, 174102 (2004).
- [3] J.D. Hart, K. Bansal, T.E. Murphy, R. Roy, Chaos **26(9)**, 094801 (2016).
- [4] K. Bansal, J.O. Garcia, S.H. Tompson, T. Verstynen, J.M. Vettel, S.F. Muldoon, Science Advances **5(4)**, 8535 (2019).
- [5] T. Chouzouris, I. Omelchenko, A. Zakharova, J. Hlinka, P. Jiruska, E. Schöll, Chaos **28**, 045112 (2018).
- [6] S. Ghosh, S. Jalan, International Journal of Bifurcation and Chaos **26(07)**, 1650120 (2016).
- [7] I. Omelchenko, Y. Maistrenko, P. Hövel, E. Schöll, Phys. Rev. Lett. **106(23)**, 234102 (2011).
- [8] B.K. Bera, D. Ghosh, M. Lakshmanan, Phys. Rev. E **93(1)**, 012205 (2016).
- [9] S.R. Ujjwal, R. Ramaswamy, Phys. Rev. E **88(3)**, 032902 (2013).
- [10] C. Meena, K. Murali, S. Sinha, International Journal of Bifurcation and Chaos **26(09)**, 1630023 (2016).
- [11] G. I. Strelkova, T.E. Vadivasova, V. S. Anishchenko, Regular and Chaotic Dynamics **23(7-8)**, 948960 (2018).
- [12] N. Semenova, A. Zakharova, E. Schöll, V. Anishchenko, EPL **112(4)**, 40002 (2015).
- [13] P. Kumar, D. K. Verma, P. Parmananda, Phys. Lett. A **381(29)**, 23372343 (2017).
- [14] N. Lazarides, G. Neofotistos, G. Tsironis, Phys. Rev. B **91(5)**, 054303 (2015).
- [15] E. A. Martens, S. Thutupalli, A. Fourrière, O. Hallatschek, Proceedings of the National Academy of Sciences **110(26)**, 1056310567 (2013).
- [16] S. Nkomo, M. R. Tinsley, K. Showalter, Phys. Rev. Lett. **110(24)**, 244102 (2013).
- [17] M. J. Panaggio, D. M. Abrams, Nonlinearity **28(3)**, 67 (2015).
- [18] E. Schöll, The European Physical Journal Special Topics **225(6-7)**, 891919 (2016).
- [19] D. Dudkowski, Y. Maistrenko, T. Kapitaniak, Phys. Rev. E **90(3)**, 032920 (2014).
- [20] A. Zakharova, M. Kapeller, E. Schöll, Phys. Rev. Lett. **112(15)**, 154101 (2014).
- [21] D. M. Abrams, R. Mirollo, S. H. Strogatz, D. A. Wiley, Phys. Rev. Lett. **101(8)**, 084103 (2008).

- [22] J. Xie, E. Knobloch, H. -C. Kao, Phys. Rev. E **90(2)**, 022919 (2014).
- [23] L. Schmidt, K. Krischer, Chaos **25(6)**, 064401 (2015).
- [24] C. R. Laing, Physica D: Nonlinear Phenomena **238(16)**, 15691588 (2009).
- [25] A. Schmidt, T. Kasimatis, J. Hizanidis, A. Provata, P. Hövel, Phys. Rev. E **95**, 032224 (2017).
- [26] Y. Maistrenko, O. Sudakov, O. Osiv, V. Maistrenko, New Journal of Physics **17(7)**, 073037 (2015).
- [27] T. Kasimatis, J. Hizanidis, A. Provata, Phys. Rev. E **97**, 052213 (2018).
- [28] C. R. Laing, Phys. Rev. E **92(5)**, 050904 (2015).
- [29] G. C. Sethia, A. Sen, Phys. Rev. Lett. **112(14)**, 144101 (2014).
- [30] R. G. Andrzejak, C. Rummel, F. Mormann, K. Schindler, Scientific reports **6**, 23000 (2016).
- [31] F.P. Kemeth, S. W. Haugland, L. Schmidt, I.G. Kevrekidis, K. Krischer, Chaos **26(9)**, 094815 (2016).
- [32] R. Gopal, V. Chandrasekar, A. Venkatesan, M. Lakshmanan, Phys. Rev. E **89(5)**, 052914 (2014).
- [33] M. Wolfrum, O. E. Omelchenko, S. Yanchuk, Y. L. Maistrenko, Chaos **21(1)**, 013112 (2011).
- [34] I. Omelchenko, E. Omelchenko, P. Hövel, E. Schöll, Phys. Rev. Lett. **110(22)**, 224101 (2013).
- [35] J. Hizanidis, N. E.Kouvaris, G. Zamora López, A. Díaz Guilera, C. G. Antonopoulos, Scientific reports **6**, 19845 (2016).
- [36] T. M. Mitchell, *Machine Learning*, McGraw Hill Education; First edition (2017).
- [37] A. Burkov, *The Hundred-Page Machine Learning Book*, Andriy Burkov; 1 edition (2019).
- [38] Z. Lu, B.R. Hunt, E. Ott, Chaos **28**, 061104 (2018).
- [39] J. Pathak, Z. Lu, B.R. Hunt, M. Girvan, E. Ott, Chaos **27**, 121102 (2017).
- [40] J. Pathak *et al.*, Chaos **28**, 041101 (2018).
- [41] F. A.Rodrigues *et al.*, arXiv:1910.00544 (2019).
- [42] G. Neofotistos *et al.*, Frontiers in Physics **7**, 24 (2019).
- [43] J.D. Hart, L. Larger, T.E. Murphy, R. Roy, Philos. Trans. of the Royal Society A **377(2153)**, 20180123 (2019).
- [44] M. Fernández-Delgado, E. Cernadas, S. Barro, D. Amorim, The Journal of Machine Learning Research **15(1)**, 31333181 (2014).
- [45] L. Breiman, Machine learning **45(1)**, 532 (2001).
- [46] L. Zhang, P.N. Suganthan, IEEE transactions on cybernetics **45(10)**, 21652176 (2014).
- [47] Y. Zhang, J. Wu, Z. Cai, B. Du, S.Y. Philip, Neural Networks **112**, 8597 (2019).

- [48] J. Marroquin, S. Mitter, T. Poggio, Journal of the american statistical association **82(397)**, 7689 (1987).
- [49] O. L. Mangasarian, R. Meyer, SIAM Journal on Control and Optimization **17(6)**, 745752 (1979).
- [50] T. Evgeniou, M. Pontil, T. Poggio, Advances in computational mathematics **13(1)**, 1 (2000).
- [51] L.-F. Chen, H.-Y.M. Liao, M.-T. Ko, J.-C. Lin, G.-J. Yu, Pattern recognition **33(10)**, 17131726 (2000).
- [52] Y.-H. Pao, G.-H. Park, D.J. Sobajic, Neurocomputing **6(2)**, 163180 (1994).
- [53] S. Ghosh, L. Schülen, A. D. Kachhvah, A. Zakharova, S. Jalan, EPL **127**, 30002 (2019).
- [54] Y. Kuramoto, *Lecture Notes in Physics, International Symposium on Mathematical Problems in Theoretical Physics*. H. Araki (ed.) **39**, 420 Springer-Verlag, New York (1975).
- [55] S. Strogatz, Physica D **143 (14)**, 120 (2000).
- [56] F. A. Rodrigues, T. K. Peron, P. Jie, J. Kurths, Physics Reports **610 (1)**, 198 (2016).
- [57] S. Jalan, S. Ghosh, B. Patra, Chaos **27**, 101104 (Fast Track) (2017).
- [58] M. Masoliver, N. Malik, E. Schöll, A. Zakharova, Chaos **27**, 101102 (2017).
- [59] N. Semenova, A. Zakharova, V. S. Anishchenko, E. Schöll, Phys. Rev. Lett. **117**, 014102 (2016).
- [60] L. Schülen, S. Ghosh, A.D. Kachhvah A.D., A. Zakharova, S. Jalan, Chaos, Solitons and Fractals **128**, 290296 (2019).
- [61] R. May, Nature **261 (5560)**, 459467 (1976).
- [62] E. Ott, *Chaos in dynamical systems*, Cambridge University Press (1993).
- [63] S. Jalan *et al.*, Phys. Rev. E. **94**, 062202 (2016); F. M. Atay, J. Jost, A. Wende, Phys. Rev. Lett. **92**, 144101 (2004); N. K. Pareeka *et al.*, Image Vision Comput. **24**, 926 (2006); S.C. Phatak, S.S. Rao, S.S., Phys. Rev. E **51**, 3670 (1995); H. Gang, Q. Zhilin, Phys. Rev. Lett. **72**, 68 (1994); N. Parekh, S. Parthasarathy, S. Sinha, Phys. Rev. Lett. **81**, 1401 (1998).
- [64] M. Hénon, Communications in Mathematical Physics **50 (1)**, 6977 (1976).
- [65] U. Lee *et al.*, Scientific Reports **8**, 243 (2018).
- [66] V.A. Maksimenko, Phys. Rev. E **96**, 012316 (2017)
- [67] A. Palmigiano, J. Pastor, R. García de Sola, G.J. Ortega, PLoS ONE **7(7)**, e41799 (2012).
- [68] I. Kanter *et al.*, EPL **93**, 66001 (2011).
- [69] A. Singh, S. Jalan, S. Boccaletti, Chaos **27**, 043103 (2017).
- [70] B. Blasius, A. Huppert, L. Stone, Nature **399(6734)**, 354-9 (1999).